Journal of Applied Physics

Role of graphite on the thermoelectric performance of Sb_2Te_3/graphite nanocomposite

Cite as: J. Appl. Phys. **125**, 195105 (2019); https://doi.org/10.1063/1.5095935
Submitted: 13 March 2019 . Accepted: 28 April 2019 . Published Online: 21 May 2019

Subarna Das, P. Singha, A. K. Deb, S. C. Das, S. Chatterjee, V. A. Kulbachinskii, V. G. Kytin, D. A. Zinoviev, N. V. Maslov, Sandip Dhara, S. Bandyopadhyay, and Aritra Banerjee

Journal of Applied Physics ARTICLE scitation.org/journal/jap

Role of graphite on the thermoelectric performance of Sb_2Te_3/graphite nanocomposite

Cite as: J. Appl. Phys. **125**, 195105 (2019); doi: 10.1063/1.5095935
Submitted: 13 March 2019 · Accepted: 28 April 2019 ·
Published Online: 21 May 2019

View Online Export Citation CrossMark

Subarna Das,[1] P. Singha,[1] A. K. Deb,[2] S. C. Das,[3] S. Chatterjee,[3] V. A. Kulbachinskii,[4] V. G. Kytin,[4] D. A. Zinoviev,[4] N. V. Maslov,[4] Sandip Dhara,[5] S. Bandyopadhyay,[1,6] and Aritra Banerjee[1,6,a)]

AFFILIATIONS

[1]Department of Physics, University of Calcutta, 92 A P C Road, Kolkata 700 009, India
[2]Department of Physics, Raiganj University, Uttar Dinajpur, West Bengal 733 134, India
[3]UGC-DAE Consortium for Scientific Research, Kolkata Centre, Sector III, LB-8, Salt Lake, Kolkata 700 098, India
[4]Department of Low Temperature Physics and Superconductivity, Physics Faculty, M.V. Lomonosov Moscow State University, Moscow 119991, Russia
[5]Surface and Nanoscience Division, Indira Gandhi Centre for Atomic Research, Homi Bhabha National Institute, Kalpakkam 603 102, India
[6]Center for Research in Nanoscience and Nanotechnology, University of Calcutta, JD-2, Sector-III, Saltlake, Kolkata 700 106, India

[a)]**Author to whom correspondence should be addressed:** arbphy@caluniv.ac.in

ABSTRACT

Thermoelectric properties of nanostructured Sb_2Te_3/graphite composites are investigated both experimentally and theoretically and the contribution of graphite to heat transport mechanism is addressed. XRD results indicate the solid state insolubility of the graphite phase in Sb_2Te_3 as no shift is observed in the diffraction peaks corresponding to Sb_2Te_3 in the composite samples. Raman spectroscopic analysis confirms the presence of graphite in the nanostructured composite samples. Temperature dependence of carrier concentration n_H, thermal conductivity κ, Seebeck coefficient S, resistivity ρ, and, hence, the thermoelectric figure of merit ZT is reported. Graphite incorporation leads to around 40% decrease of κ, essentially due to the decrease of lattice thermal conductivity, κ_L. A low κ_L value of 0.8 $Wm^{-1}K^{-1}$ is reported, which mostly arises due to enhanced phonon scattering at the heterointerfaces created by the addition of graphite. S increases in Sb_2Te_3/graphite nanocomposites. Calculation reveals that reported large S value is related with the low hole concentration. Theoretical simulation in the frame of Boltzmann equation approach shows satisfactory agreement of n_H, S, and ρ with experimental data, and based on the modification of the density of states and its derivative near Fermi energy with graphite addition, a plausible explanation is provided.

I. INTRODUCTION

A thermoelectric (TE) material is a promising platform for converting waste thermal energy into valuable electrical energy and hence attracts wide research interest in Condensed Matter and Material Physics.[1] Over the past few decades, it has drawn attention of researchers immensely due to its potential to be viable as a green energy source. Efficient TE materials could enable the replacement of compression based refrigeration system as well. These application potentials lead to the resurgence in activity toward obtaining a TE material with better efficiency. Efficiency of a TE material is designated by a dimensionless term figure of merit, $ZT = \frac{S^2}{\rho\kappa}T$, where ρ is the electrical resistivity, S is the Seebeck coefficient (or thermopower), κ is the thermal conductivity, and T is the absolute temperature. The parameters, i.e., S, ρ, and κ, are interrelated. Therefore, it has been a great challenge for years to obtain high ZT TE materials.[2–5] It is thus imperative to decouple these parameters.[6] From this viewpoint, there are two representative methods for enhancing ZT: nanostructuring as an intrinsic method and composite as an extrinsic method.[7–12] Nanostructuring leads to low κ due to increased phonon scattering at the nanograin boundaries.[13,14] However, at the same time, carrier (electron/hole) scattering at the nanograin boundary increases ρ, which is undesirable. Composites, another promising method to obtain high ZT material, consist of TE matrix and nanosized dispersoids.[15–18] In the composite

TE material, interface scattering plays a significant and a positive role. Hicks and Dresselhaus also proposed to introduce quantum confinement effects in low dimension materials, by introducing nanoscale phase into the TE matrix.[15,19,20] The enhanced interface scattering at the newly formed boundaries between TE matrix and nanoscale disperoids reduces κ to a great extent.[11,21,22] Moreover, the nanograin boundaries in composites increase S by means of carrier filtering or quantum confinement effect, although ρ of these highly disordered material is usually compromised.[23–25]

Binary pnictide chalcogenides, viz., Bi_2Te_3 (both n and p-type) and Sb_2Te_3 (p-type) are well known TE materials near room temperature (RT).[26–28] Their layered crystal structure leads to a poor κ, suitable for TE applications.[29] Carbon based materials provide phonon blocking.[10,21,22] Hence, as second phase carbon based materials, viz., graphene and carbon nanotube (CNT) have been a popular choice, where its high electrical conductivity also plays a positive role.[30] Graphene nanosheets have been reported to be effective in enhancing the TE performance of polyaniline (PANI) based TE nanocomposite samples.[31] In recent years, the influence of CNT, graphene, and graphite on the TE properties of Bi_2Te_3 based nanostructured composite samples has been extensively studied.[10,11,32–34] Another important related pnictide chalcogenide TE material is $Bi_{0.5}Sb_{1.5}Te_3$. It has been reported that formation of nanocomposite of $Bi_{0.5}Sb_{1.5}Te_3$ with graphite and C_{60} effectively reduces κ.[21,22,35] Simultaneous increase in electrical conductivity and phonon scattering in the graphene nanosheet/$(Bi_2Te_3)_{0.2}(Sb_2Te_3)_{0.8}$ TE nanocomposite has also been reported by Li *et al.*[36] Despite such attempts, it should be mentioned that only limited efforts have been made to study the TE performance of p-type Sb_2Te_3 based nanocomposite system.[37–39] However, to the best of our knowledge, the effect of dispersing carbon based compounds on the TE properties of the Sb_2Te_3 composite system is yet to be explored.

In this article, the TE properties of the Sb_2Te_3/graphite nanocomposite system have been studied in detail. A high room temperature (RT) S value of around 210 μV/K is obtained for the pristine nanostructured Sb_2Te_3 sample, which further increases to around 250 μV/K with 1.0 wt. % of graphite. The obtained S is one of the highest values reported for Sb_2Te_3 based samples. In addition, a 40% reduction in κ near RT is observed in the synthesized Sb_2Te_3/graphite nanocomposites. Furthermore, the experimental data are theoretically simulated in the framework of Boltzmann equation approach for isotropic dispersion law. Quantitative agreement between calculation and experimental data is obtained. The modification of the electronic states with graphite incorporation is predicted from the theoretical modeling.

II. EXPERIMENTS

Polycrystalline Sb_2Te_3 ingots were synthesized by solid state reaction method, details of which could be obtained elsewhere.[26,28] Corresponding nanocomposite samples, i.e., Sb_2Te_3 + x wt. % graphite (x = 0, 0.5, and 1.0), were prepared subsequently by adding desired weight percentage of graphite with the synthesized Sb_2Te_3 ingots using planetary ball mill machine (Pulverisette, Fritsch, Germany). The speed of main disk was 200 rpm and the ball to sample ratio of 10:1 was used during milling. To avoid any unwanted reaction, especially oxidation, milling was performed in Ar atmosphere. Ball milled powders were pressed into pellets using the hot press method under the uniaxial pressure of 70 MPa at 425 °C (698 K) temperature for 1 h. The pellets thus obtained had a density of around 90% of the theoretical density of pristine Sb_2Te_3 (6.50 g/cm^3). Structural characterization of Sb_2Te_3 + x wt. % graphite (x = 0, 0.5, and 1.0) samples were carried out using synchrotron powder X-ray diffraction (XRD) facility at the Indian Beamline BL-18B, Photon Factory, Japan. The samples were illuminated by a monochromatic X-ray beam with wavelength $\lambda = 0.09782$ nm. Synchrotron powder XRD measurements were performed in the $10° \leq 2\theta \leq 50°$ range. Standard Si was used to determine the instrumental profile.[40] Rietveld refinement technique using MAUD software was employed to extract the structural parameters for all the samples.[41] Microstructures of the samples were characterized using Transmission Electron Microscope (TEM; JEM 2100 HR, JEOL) operating at 200 KV. Details of ρ(T),[26,42] S(T),[26,42] κ(T),[43] Hall coefficient n_H(T) measurements,[44] and room temperature Raman spectroscopic studies[26,28,45] can be found elsewhere.

III. RESULTS AND DISCUSSION

Figure 1 represents XRD patterns after Rietveld refinement of Sb_2Te_3 + x wt. % graphite (x = 0, 0.5, and 1.0) nanocomposite samples. All the diffraction peaks are indexed with the rhombohedral crystal structure of Sb_2Te_3 with space group $R\bar{3}m$. No additional peak is evidenced due to the graphite phase in the synthesized nanocomposite samples. The amount of graphite added is very small, at least within the detection limit of XRD.[33,36] However, existence of graphite is confirmed by Raman spectra (RS) as shown later. At the same time, XRD results clearly indicate the solid state insolubility of graphite in Sb_2Te_3 as no shift is observed in the diffraction peaks of nanocomposite samples. Rietveld refinement details along with the parameters obtained after refinement are provided in Table SM1 in the supplementary material. The extracted unit cell parameters of the Sb_2Te_3/graphite nanocomposite samples are also presented in Table I. It is revealed that lattice parameters do not significantly change with the addition of graphite. Also, grain sizes of all the nanocomposite samples, as obtained after refinement, are around 15 nm (see Table SM1 in the supplementary material). This excludes grain size and related other effects on ρ(T), S(T), κ(T), and n_H(T) data as well as TE properties of synthesized Sb_2Te_3/graphite nanocomposite.

Raman spectroscopic measurement confirms the presence of graphite in Sb_2Te_3/graphite nanocomposite samples (Fig. 2). The primitive unit cell of Sb_2Te_3 contains 5 atoms giving rise to 15 lattice dynamical modes at the center of the Brillouin zone, among which 3 are acoustic modes and 12 are optical modes. Because of inversion symmetry, these optical modes are exclusively Raman or infrared active. Out of these 12 optical modes, 4 modes, e.g., $2A_{1g}$, $2E_g$ are Raman active in the frequency range of 30–200 cm^{-1} and $2A_{1u}$, $2E_u$ are infrared (IR) active. More detailed analysis along with the corresponding atomic displacements for different vibrational modes can be found in the literature.[25,46] In Fig. 2, peaks observed at around 64 and 117 cm^{-1} are attributed to Raman active A^1_{1g} and E^2_g vibrational modes of Sb_2Te_3, respectively.[44–48] The peak at 135 cm^{-1} indicates the IR active mode of Sb_2Te_3.[49] The IR active mode in Raman spectra mostly arises due to the breakdown of

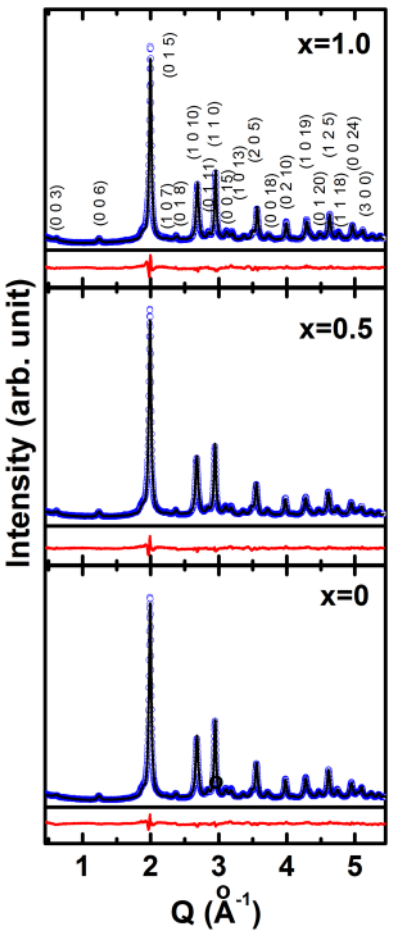

FIG. 1. X-ray diffraction patterns of Sb_2Te_3 + x wt. % graphite (x = 0, 0.5, and 1.0) samples at room temperature after Rietveld refinement.

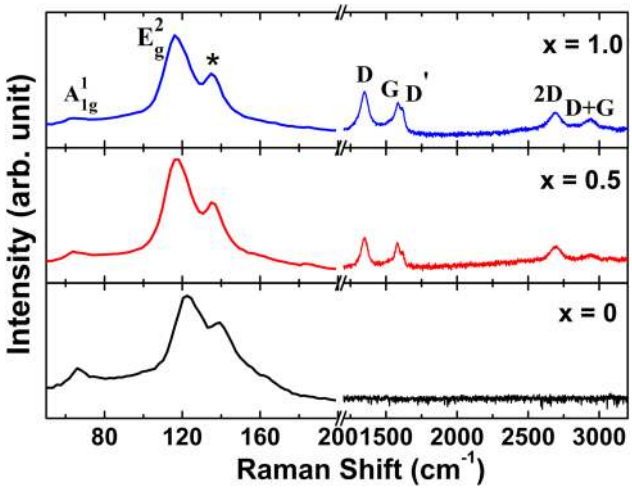

FIG. 2. Room temperature Raman spectra of Sb_2Te_3 + x wt. % graphite (x = 0, 0.5, and 1.0) nanocomposites. Raman active A_{1g}^1 and E_g^2 mode of Sb_2Te_3 are indicated. The peak marked with asterisk (*) is associated to the IR active mode of Sb_2Te_3. Raman active D, G, D′, 2D, and D + G bands confirm the presence of graphite in x = 0.5 and 1.0 samples.

crystal symmetry as a finite size effect in nanostructured samples and has been reported earlier by Shahil *et al.* during Raman spectroscopic analysis of mechanically exfoliated few-quintuple layers of Bi_2Te_3.[47] In addition, all the as-prepared Sb_2Te_3/graphite composite samples exhibit several Raman active peaks: *D* band (~1350 cm^{-1}) and *D′* band (~1620 cm^{-1}) corresponding to defect and disorder induced or edge areas of graphite and *G* band (~1580 cm^{-1}), arising due to vibration of sp^2-hybridized carbon.[50] The peak at about 2950 cm^{-1} is also induced by disorder and associated with *D* + *G* combination mode. Furthermore, the Raman band appearing around 2700 cm^{-1} corresponds to the overtone of the *D* band (*2D*), which arises due to the double resonant scattering process from the zone edge phonons of graphite and is exhibited in all kinds of graphitic materials.[51]

The presence of graphite and nature of its distribution are further confirmed by TEM study. High resolution TEM image of a typical Sb_2Te_3/graphite composite sample with highest graphite concentration (x = 1.0) is illustrated in Fig. SM1 in the supplementary material. Several lattice stripes with definite widths of 0.322 nm, 0.272 nm, and 0.210 nm clearly represent, respectively, the (015), (018), and (110) planes of Sb_2Te_3. Some less dark regions, identified as graphite (marked by a dotted circle in Fig. SM1 in the supplementary material), indicate that graphite is randomly dispersed in the Sb_2Te_3 matrix.

In order to investigate the TE properties of bulk Sb_2Te_3/graphite composites, κ(T), *S*(T), and ρ(T) measurements were carried out. Figure 3(a) shows the temperature dependent variation of κ for different Sb_2Te_3/graphite composite samples. The room temperature κ value (~1.5 Wm^{-1}K^{-1}) of pristine Sb_2Te_3 is in excellent agreement with the reported data.[39] As demonstrated in Fig. 3(a), κ values of Sb_2Te_3/graphite composites significantly decrease compared to those of the pristine Sb_2Te_3 sample over the whole temperature range. A maximum reduction of 40% in κ is observed for the Sb_2Te_3 composite sample containing 0.5 wt. % of graphite. The total thermal conductivity (κ) is composed of electronic contribution (κ_e) from the charge carriers and lattice contribution (κ_L) from phonons: $\kappa = \kappa_e + \kappa_L$. The contribution of κ_e can be estimated with the Wiedemann–Franz law: $\kappa_e = LT\sigma$, where *L* is the Lorentz number and σ (=1/ρ) is the electrical conductivity. Instead of common

TABLE I. Lattice parameters (*a* and *c*) extracted by Rietveld refinement of XRD patterns for Sb_2Te_3 + x wt. % graphite (x = 0, 0.5, and 1.0) samples.

x	*a* (Å)	*c* (Å)
0	4.273 6	30.422 3
0.5	4.275 6	30.441 4
1.0	4.272 4	30.343 8

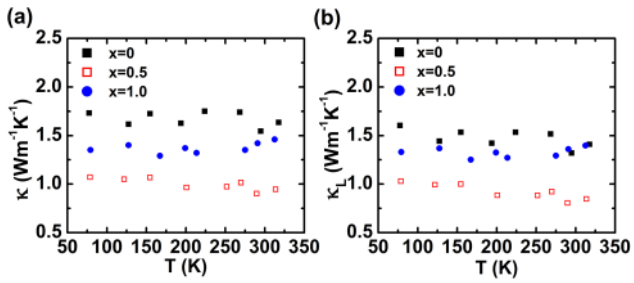

FIG. 3. Temperature dependence of (a) total thermal conductivity (κ) and (b) lattice thermal conductivity (κ_L) for Sb_2Te_3 + x wt. % graphite (x = 0, 0.5, and 1.0) samples indicating similar variation of κ(T) and κ_L(T) with graphite concentration.

practice to treat L as a universal factor with $2.44 \times 10^{-8}\,W\,\Omega\,K^{-2}$ (degenerate limit),[52] first order correction to the degenerate limit of L is estimated from the measured S(T) data.[53] Snyder *et al.* recently demonstrated the method to be accurate for common band structures/scattering mechanisms found for TE materials.[53] Thus, using the estimated values of L and measured ρ(T) data, κ_e(T) is evaluated. The temperature dependence of κ_L(T) is determined easily using the obtained κ and κ_e. The κ_L value as low as $0.8\,Wm^{-1}K^{-1}$ is obtained for the x = 0.5 sample near RT. Such a low value of κ_L can be found in some high ZT (>1) TE material, viz., doped PbTe, $Bi_{0.5}Sb_{1.5}Te_3/C_{60}$ nanocomposite, and others.[14,21,22] However, to the best of our knowledge, this is one of the lowest κ_L values reported for Sb_2Te_3 based samples. For comparison with κ [Fig. 3(a)], the κ_L(T) data of the composite samples as a function of graphite content are plotted in Fig. 3(b). The results reveal that κ is dependent primarily on κ_L and shows similar temperature and graphite content dependence. Therefore, the dominant factor that determines κ of Sb_2Te_3/graphite composites is the scattering of phonons.[11,32] The main cause of the reduction in κ as well as κ_L is likely the newly formed Sb_2Te_3/graphite heterointerfaces, which act as effective phonon scattering centers. The nanostructure of Sb_2Te_3 scatters heat carrying phonons. Moreover, the distributed graphite in the matrix acts as centers to scatter heat carrying phonons, and the large number of mesoscale boundaries between the two phases can also increase the scattering of phonons, which results in a decrease of κ_L and hence κ.

Due to the large difference in atomic mass between C atoms and atoms of Sb and Te, graphite nanoparticles and interfaces act as effective scattering centers of phonons in nanocomposite Sb_2Te_3. This plausibly explains the observed significant reduction of κ_L for the x = 0.5 wt. % graphite sample. However, further addition of graphite (1.0 wt. %) raises the κ values of the composite. It is noteworthy to mention that the theoretical κ value of graphite at room temperature is around 398 W/m K (for in-plane, i.e., *ab* directions) and 2.2 W/m K (for the *c* direction).[54] The observed increase in κ in the 1.0 wt. % graphite content sample can be attributed to this high κ of graphite, which subdues the reduction in κ arising due to phonon scattering effect as observed in the lower graphite (0.5 wt. %) content sample.[32] However, interestingly, all Sb_2Te_3/graphite composites have lower κ than the pristine Sb_2Te_3. Similar results are recently reported for Bi_2Te_3/graphene and Bi_2Te_3/CNT based composite TE materials.[11,32]

The Seebeck coefficients (S) of Sb_2Te_3/graphite composites are presented in Fig. 4(a). The S(T) data reveal that all samples are *p*-type in nature. The S value of the single crystalline Sb_2Te_3 compound is reported around $80\,\mu VK^{-1}$ along the cleavage planes[55] and $95\,\mu VK^{-1}$ along the perpendicular direction at 300 K.[56] However, the obtained S value of the present polycrystalline nanostructured Sb_2Te_3 samples, having average grain size around 15 nm, is much higher ($\sim 210\,\mu\,VK^{-1}$) and corroborates with the Sb_2Te_3 nanoparticle system reported earlier.[37,57,58] A similar high value of S for the Sb_2Te_3 system has also been reported by other groups.[59–63] It is noteworthy to mention that grain size of the nanostructured Sb_2Te_3 samples reported here is comparable to the de Broglie wavelength of Sb_2Te_3 (~18 nm).[58] Due to this, density of states and the energy spectrum of holes are modified. This can, in principle, decrease the carrier concentration. Nanostructuring also increases the number of grain boundaries in the system. Hence, the probability of both carrier and phonon scattering increases, which is reported to be favorable for increase of S.[15,25] Furthermore, S(T) data clearly show that addition of graphite leads to the increase of the S value of

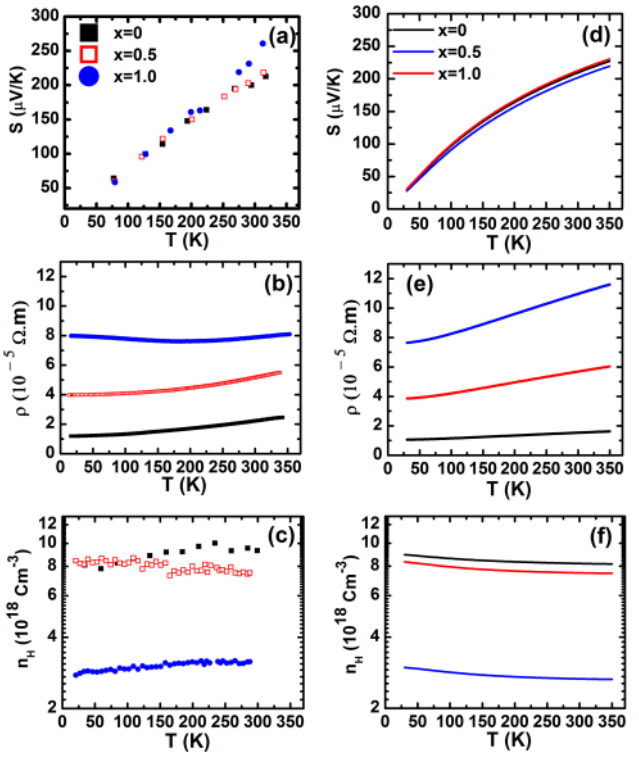

FIG. 4. Thermal variation of (a) Seebeck coefficient (S), (b) electrical resistivity (ρ), and (c) carrier concentration (n_H) for different weight percentages (x) of graphite in Sb_2Te_3/graphite nanocomposites. Figures 4(d)–4(f) represent the theoretically simulated curve of S, ρ, and n_H for the samples, respectively. The simulation was performed in the frame of the Boltzmann equation and shows satisfactory agreement with experimental data.

the composite samples. In fact, Hall measurement data discussed later indicate that carrier concentration (n_H) in Sb_2Te_3/graphite composites decreases with the addition of graphite [Fig. 4(e)]. For degenerated systems, in reference to the relatively simple semiclassical Mott Jones formula of electron transport applicable for Sb_2Te_3 and related samples, Seebeck coefficient is represented by[2]

$$S = \frac{8\pi^2 k_B^2}{3eh^2} m^* T \left(\frac{\pi}{3n_H}\right)^{\frac{2}{3}}, \quad (1)$$

where k_B is the Boltzmann constant, h is the Planck constant, m^* is the effective mass, and n_H is the carrier (hole) concentration. As demonstrated below, this also corroborates with our modeling in the framework of the kinetic equation. So, incorporation of graphite in the Sb_2Te_3/graphite composite system has a positive effect on κ and S.

The ρ(T) curve, presented in Fig. 4(b), depicts that ρ of the synthesized nanocomposite system increases with increasing graphite content. The increase in the ρ value of Sb_2Te_3/graphite samples with the increase of graphite can be mainly attributed to the decrease of n_H, since $\rho = \frac{1}{n_H e\mu}$, where μ is the carrier mobility and other symbols have their usual meaning. Furthermore, increased number of interfaces and grain boundaries resulting in additional scattering centers for carriers also lead to an observed higher ρ value in the composite samples.

For crystalline material, n_H and μ play crucial role in determining the S and ρ data as well as modulating its TE performance.[2] Thus, to have a better understanding, Hall measurements of the nanocomposite samples were performed. The measured values of n_H are relatively small compared to Sb_2Te_3 single crystals and is almost temperature independent [Fig. 4(e)].[9,64] Such behavior is rather typical for semiconductors with a single type of carriers. However, in reference to the energy band diagram proposed for Sb_2Te_3 based materials, it can be assumed that in the investigated materials, only the upper valence band (UVB) of light holes is contributing to hole transport.[21,22] In the case of contribution from the filled lower valence band (LVB) of heavy holes, redistribution of carriers between UVB and LVB takes place leading to the visible change in temperature dependence of n_H due to a large difference of hole mobilities in UVB and LVB.

We calculated the values of difference between the top of valence band E_V and Fermi energy E_F (Table II) in the degeneration limit using the experimental values of n_H and light hole effective mass tensor,[65]

$$E_V - E_F = \frac{\pi^{4/3}\hbar^2 n_H^{2/3}}{2^{5/3}(m_1 m_2 m_3)^{1/3}}, \quad (2)$$

TABLE II. The parameters of the investigated nanocomposites obtained by using the experimental n_H data at 50 K.

x	n_H (10^{18}/cm^3)	μ (cm^2/V s)	E_F (meV)	l (nm)	λ (nm)
0	8	710	24	16	19
0.5	8	200	24	4.5	19
1.0	2.8	280	12	4.4	26

where m_1, m_2, and m_3 are the components of effective mass tensor along principal directions of the valley and $\hbar$ is the Planck constant. These values are smaller than the separation between upper and lower valence bands.[21] The observed smaller value is consistent with the suggestion that only upper valence band contributes to hole transport. Furthermore, we estimated mean free path l and wavelength λ of holes from μ and E_F as shown in Table II. To obtain this, we assume isotropic and quadratic dispersion law for holes with effective mass m equal to one valley density of states effective mass,[66,67]

$$l = \frac{\mu}{e}\sqrt{2m(E_V - E_F)}, \quad \lambda = \frac{2\pi\hbar}{\sqrt{2mE_F}}, \quad m = (m_1 m_2 m_3)^{1/3}, \quad (3)$$

where e is the elementary charge.

For a sample with 0 wt. % graphite, calculated l is very close to the mean crystalline size obtained from XRD and TEM data. Thus, for this sample, n_H and ρ data suggest that hole transport is mainly limited by interface scattering and the hole mean free path is nearly independent on energy and temperature.

To verify the supposition, we calculated ρ, n_H, and S for the sample with 0 wt. % graphite in the framework of the Boltzmann equation in relaxation time approximation. In the calculation, we assume constant mean free path equal to the value in Table II. The following expressions were used:[66,67]

$$\begin{aligned}
\rho &= 1/\sigma, \\
S &= \sigma_S/\sigma, \\
n_H &= \frac{\sigma^2}{e\sigma_H}, \\
\sigma &= \frac{4e^2 lm}{\pi^2\hbar^3}\int_{-\infty}^{E_V}\frac{\partial f_0}{\partial E}(E_V - E)dE, \\
\sigma_S &= \frac{4elm}{\pi^2\hbar^3}\int_{-\infty}^{E_V}\frac{\partial f_0}{\partial T}(E_V - E)dE, \\
\sigma_H &= \frac{4\sqrt{2}e^3 l^2\sqrt{m}}{\pi^2\hbar^3}\int_{-\infty}^{E_V}\frac{\partial f_0}{\partial E}\sqrt{E_V - E}dE.
\end{aligned} \quad (4)$$

Carrier concentration was determined using the equation for concentration of acceptor impurities,[66,67]

$$N_A = \frac{6\sqrt{2}m^{3/2}}{\pi^2\hbar^3}\int_{-\infty}^{E_V} f_0\sqrt{E_V - E}dE, \quad (5)$$

where $f_0 = \frac{1}{\exp\left(\frac{E_F - E}{k_B T}\right)+1}$, k_B is the Boltzmann constant, T is the temperature, and N_A is the concentration of ionized acceptors that we assumed to be temperature independent. We also assumed that all acceptors are ionized. Using the concentration of carriers, we can calculate Fermi energy. The only fitting parameter was N_A. Effective mass $m = 0.184m_0$ was calculated using expression (2) and data provided in Ref. 65, where m_0 is the mass of free electron.

We can observe (Fig. 4) that the temperature dependencies of S, n_H, and ρ are in good agreement with experimental data. The difference in temperature variation of ρ and n_H can originate from hole scattering by phonons. Thus, hole transport can be described in the frame of the Boltzmann equation, although hole wavelength is comparable to the hole mean free path and hole momentum is not a good quantum number. However, expression (4) can hold their validity if electronic states near the top of valence band remain delocalized. Every electron state carries probability flux density i. Nonequilibrium energy distribution function of holes over states carrying i has the same form as for Bloch states in the crystalline material, where $i = \frac{p}{m}$. Hence, the density of states has the same form of the crystalline material and determined by m and valley degeneration, which is equal to 6 for Sb_2Te_3.

In the nanocrystalline material, electronic states near the top of valence band form the electronic Bloch states of crystallites. Therefore, the density of states could uphold its energy dependence and the above-mentioned other conditions could be fulfilled. In this case, our calculation shows that the large value of S in the crystalline material originates from relatively low hole concentration.

Assuming that the applicability of expressions (3–4) holds also for nanocomposite samples with graphite, we make an attempt to fit temperature dependencies of S, ρ, and n_H using two fitting parameters: N_A and m and taking l equal to estimates from Table II. The calculated values of the temperature dependencies of the S, ρ, and n_H are shown in Figs. 4(d)–4(f), respectively, and are in reasonable quantitative agreement with experimental data. The list of calculated parameters is given in Table III.

For a sample with 0.5 wt. % graphite, the optimal value of effective mass is very close to the literature value used for the sample with 0 wt. % graphite content. The value of ionized acceptor concentration is slightly smaller. Thus, the effect of 0.5 wt. % graphite on electronic states and carrier concentration is negligible. The significant effect is the acceleration of the relaxation of distribution function, which is indicated by essentially a smaller value of l. The fast relaxation of distribution function can be due to weak coupling of electronic states in graphite particles with electronic states near the top valence band in Sb_2Te_3.

For sample with 1.0 wt. % graphite, optimal N_A is significantly smaller than those in 0 wt. % and 0.5 wt. % graphite content samples. This smaller N_A value points to the localization of the part of charge carriers. Thermal activation of these carriers to the delocalized states could explain the difference between experimental and calculated S for the sample with 1.0 wt. % graphite. Additionally, the optimal value of m is essentially smaller in this sample than in the samples with 0 wt. % and 0.5 wt. % graphite content. This points to the smaller density of electronic states and its derivative near Fermi energy for the sample with x = 1.0. Modification of energy spectrum with larger graphite content could explain the smaller concentration of charge carriers. Significant amount of carriers could be captured by graphite particles in this sample (x = 1.0) due to the change of energy difference between acceptor defects and electronic states in graphite particles. Thus, addition of 1.0 wt. % graphite modifies electronic states and their distribution in Sb_2Te_3 nanocrystalline material. Experimentally measured S for all samples is almost the same below 250 K. It is consistent with the results of our calculation. This indicates that the lower concentration of charge carriers in the sample with 1.0 wt. % graphite is compensated by modification of energy spectrum.

TABLE III. Parameters used to calculate temperature dependence of n_H, S, and ρ.

x	m/m_0	N_A (10^{18}/cm^3)
0	0.184 (calculated)	9.1 (fitted)
0.5	0.181 (fitted)	8.4 (fitted)
1.0	0.085 (fitted)	3.0 (fitted)

The room temperature ZT value for the synthesized samples varies between 0.38 (x = 0) and 0.18 (x = 1.0) and increases with increasing temperature (see Fig. SM2 in the supplementary material). It is noteworthy to mention that graphite addition plays a positive role toward the betterment of crucial TE parameters, i.e., S and κ. However, the positive effect in S and κ data is subdued by the increase of ρ with graphite addition in Sb_2Te_3/graphite nanocomposite samples, which in turn is reflected in the ZT values.

In this work, we evaluate the role of graphite in the Sb_2Te_3/graphite nanocomposite system both experimentally and theoretically, and the contribution of graphite in heat transport is emphasized. It should be pointed that graphite addition simultaneously improves crucial TE parameters, viz., κ and S, which makes the present study interesting. The enhanced TE property can be expected by applying this approach to prepare a similar nanocomposite system with graphite dispersion, and tuning of graphite concentration and related TE material/graphite nanocomposites should be investigated in future.

IV. CONCLUSION

The phase purity of the Sb_2Te_3 + x wt. % graphite (x = 0, 0.5, and 1.0) nanocomposite samples, synthesized by the ball milling method, is confirmed by XRD studies. Rietveld refinement, carried out based on the XRD data, reveals that the lattice parameters as well as the grain size of the synthesized samples do not change significantly with graphite concentration. Raman spectroscopic analysis and transmission electron microscopy confirm the presence of graphite in the sample. S value as high as 212 μV/K is obtained for pristine nanostructured Sb_2Te_3. Seebeck coefficient, Hall carrier concentration, and resistivity of investigated samples were calculated using expressions derived from the Boltzmann equation for isotropic dispersion law and constant mean free path. Reasonable quantitative agreement between calculation and experimental data was obtained with only one (for x = 0) or two (for x = 0.5 and 1.0) fitting parameters. Calculations show that the high S value of pristine Sb_2Te_3 originates mainly from lower carrier concentration. Variation of fitting parameters points to the acceleration of relaxation of the hole distribution function for an addition of 0.5 wt. % graphite. Significant modification of electronic states including reduction of the density of states and its derivative near Fermi energy is also demonstrated with graphite incorporation. In addition, modeling depicts localization of the part of states for the 1.0 wt. % graphite content sample. Graphite incorporation significantly decreases κ of nanostructured composite samples. In order to calculate κ_L accurately, first order correction to the

degenerate limit of Lorentz number L is considered for the estimation of κ_e and L is obtained from the measured S data. κ_L thus extracted from κ is found to be as low as 0.8 $Wm^{-1}K^{-1}$ in Sb_2Te_3/graphite nanocomposite. This low κ_L along with high S makes graphite a potential dispersoid in nanostructured Sb chalcogenides based TE material, which has not been reported earlier.

SUPPLEMENTARY MATERIAL

See the supplementary material for Rietveld refinement details along with the refinement parameters, high resolution TEM image of a typical nanostructured Sb_2Te_3/graphite composite sample, and temperature dependence of ZT of nanocomposite samples.

ACKNOWLEDGMENTS

Subarna Das is thankful to UGC, India for providing senior research fellowship. The authors are also grateful to Dr. S. Bhattacharya, BARC, India for providing necessary facilities (hot press) toward sample synthesis. The authors would also like to thank DST, India for the financial support and SINP, India and JNCASR, India for facilitating the experiments at the Indian Beamline, Photon Factory, KEK, Japan.

REFERENCES

[1]K. Behnia, *Fundamentals of Thermoelectricity* (Oxford University Press, Oxford, 2015).
[2]G. J. Snyder and E. S. Toberer, Nat. Mater. **7**, 105 (2008).
[3]A. I. Hochbaum, R. Chen, R. D. Delgado, W. Liang, E. C. Garnett, M. Najarian, A. Majumdar, and P. Yang, Nature **451**, 163 (2008).
[4]A. Zevalkink, D. M. Smiadak, J. L. Blackburn, A. J. Ferguson, M. L. Chabinyc, O. Delaire, J. Wang, K. Kovnir, J. Martin, L. T. Schelhas, T. D. Sparks, S. D. Kang, M. T. Dylla, G. J. Snyder, B. R. Ortiz, and E. S. Toberer, Appl. Phys. Rev. **5**, 021303 (2018).
[5]B. Beltran-Pitarch, J. Prado-Gonjal, A. V. Powell, P. Ziolkowski, and J. Garcia-Canadas, J. Appl. Phys. **124**, 025105 (2018).
[6]Y. Pan, Y. Qiu, I. Witting, L. Zhang, and C. Fu, J. W. Li, Y. Huang, F.-H. Sun, J. He, G. J. Snyder, C. Felser, and J.-F. Li, Energy Environ. Sci. **12**, 624 (2019).
[7]J.-F. Li, W.-S. Liu, L.-D. Zhao, and M. Zhou, NPG Asia Mater. **2**, 152 (2010).
[8]J. S. Son, M. K. Choi, M.-K. Han, K. Park, J.-Y. Kim, S. J. Lim, M. Oh, Y. Kuk, C. Park, S.-J. Kim, and T. Hyeon, Nano Lett. **12**, 640 (2012).
[9]V. A. Kulbachinskii, V. G. Kytin, A. A. Kudryashov, and P. M. Tarasov, J. Solid State Chem. **193**, 47 (2012).
[10]K. T. Kim, S. Y. Choi, E. H. Shin, K. S. Moon. H. Y. Koo, G.-G. Lee, and G. H. Ha, Carbon **52**, 541 (2013).
[11]Q. Zhang, L. Xu, Z. Zhou, L. Wang, W. Jiang, and L. Chen, J. Appl. Phys. **121**, 055104 (2017).
[12]V. Vargiamidis and N. Neophytou, Phys. Rev. B **99**, 045405 (2019).
[13]W. Xie, X. Tang, Y. Yan, Q. Zhang, and T. M. Tritt, Appl. Phys. Lett. **94**, 102111 (2009).
[14]K. Biswas, J. He, I. D. Blum, C.-I. Wu, T. P. Hogan, D. N. Seidman, V. P. Dravid, and M. G. Kanatzidis, Nature **489**, 414 (2012); Y. Lu, T. Sun, and D.-B. Zhang, Phys. Rev. B **97**, 174304 (2018).
[15]M. S. Dresselhaus, G. Chen, M. Y. Tang, R. Yang, H. Lee, D. Wang, Z. Ren, J.-P. Fleurial, and P. Gogna, Adv. Mater. **19**, 1043 (2007).
[16]S. Perumal, P. Bellare, U. S. Shenoy, U. V. Waghmare, and K. Biswas, Chem. Mater. **29**, 10426 (2017).
[17]M. Ibanez, Z. Luo, A. Genc, L. Piveteau, S. Ortega, D. Cadavid, O. Dobrozhan, Y. Liu, M. Nachtegaal, M. Zebarjadi, J. Arbiol, M. V. Kovalenko, and A. Cabot, Nat. Commun. **7**, 10766 (2016).
[18]T. Mori, Small **13**, 170201 (2017).
[19]L. D. Hicks and M. S. Dresselhaus, Phys. Rev. B **47**, 12727 (1993).
[20]L. D. Hicks, T. C. Harman, X. Sun, and M. S. Dresselhaus, Phys. Rev. B Condens. Matter **53**, R10493 (1996).
[21]V. D. Blank, S. G. Buga, V. A. Kulbachinskii, V. G. Kytin, V. V. Medvedev, M. Y. Popov, P. B. Stepanov, and V. F. Skok, Phys. Rev. B **86**, 075426 (2012).
[22]V. A. Kulbachinskii, V. G. Kytin, M. Y. Popov, S. G. Buga, P. B. Stepanov, and V. D. Blank, J. Solid State Chem. **193**, 64 (2012).
[23]B. Poudel, Q. Hao, Y. Ma, Y. Lan, A. Minnich, B. Yu, X. Yan, D. Wang, A. Muto, D. Vashaee, X. Chen, J. Liu, M. S. Dresselhaus, G. Chen, and Z. F. Ren, Science **320**, 634 (2008).
[24]J. Martin, L. Wang, L. Chen, and G. S. Nolas, Phys. Rev. B **79**, 115311 (2009).
[25]A. Soni, Y. Shen, M. Yin, Y. Zhao, L. Yu, X. Hu, Z. Dong, K. A. Khor, M. S. Dresselhaus, and Q. Xiong, Nano Lett. **12**, 4305 (2012).
[26]D. Das, K. Malik, A. K. Deb, S. Dhara, S. Bandyopadhyay, and A. Banerjee, J. Appl. Phys. **118**, 045102 (2015).
[27]S. I. Kim, K. H. Lee, H. A. Mun, H. S. Kim, S. W. Hwang, J. W. Roh, D. J. Yang, W. H. Shin, X. S. Li, Y. H. Lee, G. J. Snyder, and S. W. Kim, Science **348**, 109 (2015).
[28]D. Das, S. Das, P. Singha, K. Malik, A. K. Deb, A. Bhattacharya, V. A. Kulbachinskii, R. Basu, S. Dhara, S. Bandyopadhyay, and A. Banerjee, Phys. Rev. B **96**, 064116 (2017).
[29]D. Bessas, I. Sergueev, H.-C. Wille, J. Perßon, D. Ebling, and R. P. Hermann, Phys. Rev. B **86**, 224301 (2012).
[30]X. Gu, Y. Wei, X. Yin, B. Li, and R. Yang, Rev. Mod. Phys. **90**, 041002 (2018).
[31]Y. Du, S. Z. Shen, W. Yang, R. Donelson, K. Cai, and P. S. Casey, Synth. Met. **161**, 2688 (2012).
[32]H. Ju and J. Kim, J. Alloys Compd. **664**, 639 (2016).
[33]K. Agarwal, V. Kaushik, D. Varandani, A. Dhar, and B. R. Mehta, J. Alloys Compd. **681**, 394 (2016).
[34]V. A. Kulbashinskii, V. G. Kytin, N. V. Maslov, P. Singha, S. Das, A. K. Deb, and A. Banerjee, Mater. Today Proc. **8**, 573 (2019).
[35]W. Hu, H. Zhou, X. Mu, D. He, P. Ji, W. Hou, P. Wei, W. Zhu, X. Nie, and W. Zhao, J. Electron Mater. **47**, 3344 (2018).
[36]C. Li, X. Qin, Y. Li, D. Li, J. Zhang, H. Guo, H. Xin, and C. Song, J. Alloys Compd. **661**, 389 (2016).
[37]M. H. Lee, K.-R. Kim, J.-S. Rhyee, S.-D. Park, and G. J. Snyder, J. Mater. Chem. C **3**, 10494 (2015).
[38]W. Zheng, P. Bi, H. Kang, W. Wei, F. Liu, J. Shi, L. Peng, Z. Wang, and R. Xiong, Appl. Phys. Lett. **105**, 023901 (2014).
[39]M. Ahmad, K. Agarwal, N. Kumari, and B. R. Mehta, Appl. Phys. Lett. **111**, 023904 (2017).
[40]J. G. M. Van Berkum, G. J. M. Sprong, T. de Keijser, R. Delhez, and E. J. Sonneveld, Powder Diffr. **10**, 129 (1995).
[41]L. Lutterotti, S. Matthies, and H. R. Wenk, in *Proceeding of ICOTOM14*, edited by J. A. Spunar (National Research Council of Canada, Ottawa, 1999), p. 1599; IUCr: Newsl. CPD **21**, 14 (1999).
[42]K. Malik, D. Das, S. Bandyopadhyay, P. Mandal, A. K. Deb, V. Srihari, and A. Banerjee, Appl. Phys. Lett. **103**, 242108 (2013).
[43]J. V. Zaikina, K. A. Kovnir, A. N. Sobolev, I. A. Presniakov, V. G. Kytin, V. A. Kulbachinskii, A. V. Olenev, O. I. Lebedev, G. V. Tendeloo, E. V. Dikarev, and A. V. Shevelkov, Chem. Mater. **20**, 2476 (2008).
[44]D. Das, K. Malik, A. K. Deb, V. A. Kulbachinskii, V. G. Kytin, S. Chatterjee, D. Das, S. Dhara, S. Bandyopadhyay, and A. Banerjee, Europhys Lett. **113**, 47004 (2016).
[45]D. Das, K. Malik, S. Das, P. Singha, A. K. Deb, V. A. Kulbachinskii, R. Basu, S. Dhara, A. Dasgupta, S. Bandyopadhyay, and A. Banerjee, AIP Adv. **8**, 125119 (2018).
[46]W. Richter, H. Kohler, and C. R. Becker, Phys. Status Solidi B **84**, 619 (1977).
[47]K. M. F. Shahil, M. Z. Hossain, V. Goyal, and A. A. Balandin, J. Appl. Phys. **111**, 054305 (2012).

[48]Y. Kim, X. Chen, Z. Wang, J. Shi, I. Miotkowski, Y. P. Chen, P. A. Sharma, A. L. L. Sharma, M. A. Hekmaty, Z. Jiang, and D. Smirnov, Appl. Phys. Lett. **100**, 071907 (2012).
[49]B. Zheng, Y. Sun, J. Wu, M. Han, X. Wu, K. Huang, and S. Feng, J. Phys. D Appl. Phys. **50**, 105303 (2017).
[50]R. Saito, M. Hofmann, G. Dresselhaus, A. Jorio, and M. S. Dresselhaus, Adv. Phys. **60**, 413 (2011).
[51]M. A. Pimenta, G. Dresselhaus, M. S. Dresselhaus, L. G. Cancado, A. Jorio, and R. Saito, Phys. Chem. Chem. Phys. **9**, 1276 (2007).
[52]N. W. Ashcroft and N. D. Mermin, *Solid State Physics* (Brooks/Cole, Pacific Grove, CA, 1976).
[53]H.-S. Kim, Z. M. Gibbs, Y. Tang, H. Wang, and G. J. Snyder, APL Mater. **3**, 041506 (2015).
[54]H. O. Pierson, *Handbook of Carbon, Graphite, Diamond and Fullerenes: Properties, Processing and Applications* (Noyes Publications, Park Ridge, NJ, 1994).
[55]P. Lostak, C. Drasar, J. Horak, Z. Zhou, J. S. Dyck, and C. Uher, J. Phys. Chem. Solids **67**, 1457 (2006).
[56]D. M. Rowe, *Thermoelectrics Handbook: Macro to Nano* (CRC Press, New York, 2006).
[57]G.-H. Dong, Y.-J. Zhu, and L.-D. Chen, J. Mater. Chem. **20**, 1976 (2010).
[58]J. Chen, T. Sun, D. H. Sim, H. Peng, H. Wang, S. Fan, H. H. Hng, J. Ma, F. Y. C. Boey, S. Li, M. K. Samani, G. C. K. Chen, X. Chen, T. Wu, and Q. Yan, Chem. Mater. **22**, 3086 (2010).
[59]G.-H. Dong, Y.-J. Zhu, and L.-D. Chen, CrystEngComm **13**, 6811 (2011).
[60]N. R. Paudel, K. A. Wieland, and A. D. Compaan, J. Mater. Sci. Mater. Electron **26**, 78 (2015).
[61]S. Heimann, S. Schulz, J. Schaumann, A. Mudring, J. Stotzel, F. Maculewicz, and G. Schierning, J. Mater. Chem. C **3**, 10375 (2015).
[62]U. Nithiyanantham, S. R. Ede, M. F. Ozaydin, H. Liang, A. Rathishkumar, and S. Kundu, RSC Adv. **5**, 89621 (2015).
[63]N. H. Trung, K. Sakamoto, N. V. Toan, and T. Ono, Materials **10**, 154 (2017).
[64]P. M. Tarasov, V. A. Kulbachinskii, and V. G. Kytin, J. Exp. Theor. Phys. **105**, 21 (2007).
[65]V. A. Kulbachinskii, Z. M. Dashevskii, M. Inoue, M. Sasaki, H. Negishi, W. X. Gao, P. Lostak, J. Horak, and A. de Visser, Phys. Rev. B **52**, 10915 (1995).
[66]B. M. Askerov, *Electron Transport Phenomena in Semiconductors* (Nauka, Moscow, 1985).
[67]M. Grundmann, *The Physics of Semiconductors: An Introduction Including Nanophysics and Applications*, 3rd ed. (Springer-Verlag, Berlin, 2016).